Chinese Chemical Letters 37 (2026) 111306

Contents lists available at ScienceDirect

Chinese Chemical Letters

journal homepage: www.elsevier.com/locate/cclet

Microstructure regulation to manifold catalysis sites of magnetic hydrochar for enhancing Fenton-like degradation of tetracycline

Zijing Guo[a], Yi Liang[a], Kaili He[a], Hongru Jiang[a], Xiang Liu[b], Congying Xu[a], Yawei Xiao[a,*], Jihui Li[a,*]

[a] Key Laboratory of Ministry of Education for Advanced Materials in Tropical Island Resources, School of Chemistry and Chemical Engineering, Hainan University, Haikou 570228, China
[b] College of Materials and Chemical Engineering, China Three Gorges University, Yichang 443002, China

ARTICLE INFO

Article history:
Received 26 November 2024
Revised 6 April 2025
Accepted 12 May 2025
Available online 13 May 2025

Keywords:
Magnetic hydrochar
Fenton-like degradation
Diverse shapes of iron species
Multiple catalysis sites
Tetracycline

ABSTRACT

Oxidative magnetization has attracted great attention as an efficient strategy for modulating physiochemical properties of magnetic biochar. In this paper, a K_2FeO_4-involving hydrothermal oxidative magnetization was explored to regulate multiple micro-structures for manufacture magnetic hydrochar (MHC) for Fenton-like degradation of tetracycline in aqueous solution. Diverse shapes of Fe_3O_4 and nano zero-valent iron (nZVI) were doped with abundant oxygen containing groups and persistent free radicals (PFRs). Multiple catalysis sites including iron species, PFRs, oxygen containing groups, and graphite defects contributed to accelerate the Fenton-like degradation with synergistic effect. Notably, MHC achieved a tetracycline removal rate of 99 % within 60 min at 50 mg/L, with a total organic carbon (TOC) removal rate of 35 %. Furthermore, after four cycles of reuse, the degradation efficiency slightly decreased to 93 %. This study highlights the potential of magnetic hydrochar with multiple catalytic sites in the effective and sustainable degradation of pollutants.

© 2025 Published by Elsevier B.V. on behalf of Chinese Chemical Society and Institute of Materia Medica, Chinese Academy of Medical Sciences.

Advanced oxidation processes have emerged as an efficient and prevailing technology for eliminating persistent novel organic pollutant in aqueous environment with high efficiency, especially for antibiotics, dyes, pesticides, and microplastics [1,2]. Fenton oxidation, an iron-catalyzed H_2O_2 oxidation, has been widely applied to degrade different organic pollutants with the advantages of simple operation, environmental friendliness, and low costs [3]. Reactive oxygen species (ROSs) including $^{\bullet}OH$, $^{\bullet}O_2^-$, and $^1O_2$ were usually generated for degrading pollutants, in which Fe^{2+}/Fe^{3+} cycle is the rating-determining step for catalyzing transformation of H_2O_2 into these ROSs [4]. However, traditional homogeneous Fenton oxidation suffers from low pH (usually pH 3) for recycling of Fe^{3+} to Fe^{2+} and generation of large amount of iron sludge residue in reaction system [5]. Instead, heterogeneous Fenton oxidation is recognized as a reliable advanced oxidation degradation with catalysis of various heterogeneous catalysts, significantly overcoming the above disadvantages [6].

Magnetic biochar is a low-cost and efficient heterogeneous catalyst for Fenton-like degradation of different contaminants with magnetically separable and tunable properties, where iron species and carbon matrix can collaborate with each other for activating H_2O_2 into ROSs with complementary characteristics [7]. Magnetic biochar was usually prepared by thermal decomposition using low covalent iron salts and diverse biomasses as precursors [8]. Magnetic iron species are generated and dispersed on carbon matrix with superior stability, contributing greatly to activating H_2O_2 into ROSs [9,10]. Meanwhile, carbon matrix can serve as catalyst for activating H_2O_2 into ROSs and accelerating Fe^{3+}/Fe^{2+} cycle by electron shutter and transfer with multifunctional micro-structures including functional groups, and persistent free radicals on carbon matrix [11,12].

Great achievement has been made to fabricate high-performance magnetic biochar with additional modifications for catalyzing Fenton-like elimination of various organic pollutants from water [13,14]. In particular, metal-doping provided a potential approach for enhancing catalysis activity by introducing additional catalysis sites, and synergistic effect can be achieved with the collaboration of iron species and carbon matrix. For instance, Mn-doped magnetic biochar was manufactured by $FeCl_3/MnCl_2$-promoted pyrolysis at 500 °C for photo-Fenton degradation of naphthalene, Fe-Mn binary oxides and carbon matrix synergistically boosted the degradation [15]. Mn-doped magnetic biochar was found to display increased catalysis activity for

* Corresponding authors.
E-mail addresses: ywxiao@hainanu.edu.cn (Y. Xiao), lijihui@hainanu.edu.cn (J. Li).

https://doi.org/10.1016/j.cclet.2025.111306
1001-8417/© 2025 Published by Elsevier B.V. on behalf of Chinese Chemical Society and Institute of Materia Medica, Chinese Academy of Medical Sciences.

Fenton-like degradation of different pollutants with hydroxylamine as a reducing agent, where Fe^{3+}/Fe^{2+} and Mn^{3+}/Mn^{2+} cycles were accelerated by reduction of hydroxylamine for activation of H_2O_2 into $^{\bullet}OH$ [16]. Additionally, multiple doping is also an efficient strategy for improving the catalytic activity of magnetic biochar. N/Cu co-doped magnetic biochar was synthesized for electro-Fenton elimination of amoxicillin at wide pH range with uniform dispersion of metal nanoparticles on surface, and N-doped carbon matrix, Cu, and Fe species collaborated for accelerating the degradation with improvement of charge transfer efficiency and electronic structure [17].

Alternatively, modulation of molecular-structures of carbon matrix also provides a feasible approach to improve the catalysis performance of magnetic biochar, as its functional groups [16], graphite, and persistent radical structures can serve as catalyst for activation of H_2O_2 and electron donor and shuttle for accelerating Fe^{3+}/Fe^{2+} cycle [18–20]. N-doping was applied to construct pyridine defects for improving catalysis performance for Fenton-like degradation of petroleum hydrocarbons in soil, where alkylphenyl was also introduced to enhance adsorption capability [21]. Evidently, less endeavor has been made to regulate micro-structures of carbon matrix for Fenton-like oxidation, especially for degradation of TC, and thereby remains to be explored. Overall, simultaneous modulation of iron and carbon components will provide an efficient approach for enhancing the catalysis performance of magnetic biochar for Fenton-like oxidation.

Oxidation is an efficient technology for modulating diverse micro-structures of carbon matrix and iron species of magnetic biochar, providing a potential method for improving catalysis performance [22]. Carbon matrix can be oxidized and oxygen-containing groups will be introduced to improve graphite, defects, and PFR structures. Meanwhile, small oxygen-rich molecules can also be generated for modulating the morphology of iron species [23]. Herein, a simple hydrothermal oxidative magnetization, using K_2FeO_4 as magnetic iron precursor and internal oxidant, was explored to modulate multiple micro-structures for preparation of high-performance magnetic hydrochar for boosting Fenton-like oxidation. Tetracycline, a typical contaminant with nonbiodegradable properties and toxicity to DNA, was selected to evaluate the catalysis activity of magnetic hydrochar in aqueous solution. Moreover, the magnetic hydrochar is applied to catalyze degradation of other pollutants including bisphenol A (BPA), sulfamethoxazole (SMX), and sulfamerazine (SMR) for examining its universality. This work targeted to develop a method for improving multiple physiochemical properties of biochar by hydrothermal oxidative magnetization for catalyzing Fenton-like degradation of tetracycline in aqueous solution.

The collected coconut fiber (CF) was sequentially rinsed by ultrapure water to remove surface impurities. After which it was baked at 60 °C until constant weight. Subsequently dried CF was smashed into power and sieved to 100 mesh. The obtained CF power (3 g) and potassium ferrate (3 g) were poured in a 50 mL flanged reactor. At the same time, 30 mL ultrapure water was added, stirred well, then the flange was tightened using screws and placed in a muffle furnace, where temperature gradually increased to 300 °C at a rate of 5 °C/min and maintained for 4 h. When the temperature in the muffle furnace dropped completely to ambient temperature, the flanged reactor was taken out and disassembled. The mixture obtained above is filtered to separate each other. In addition, the solid powder left behind was sequentially washed with ethanol and ultrapure water until filtrate was clear and transparent. Put it into the oven at 60 °C, dry it completely, and stored in sample bottle for spare.

Using tetracycline as model pollutant, the catalysis performance of the MHC was tested for Fenton-like degradation in aqueous solution. All experiments were performed in a 500 mL Erlenmeyer flask with 280 r/min at 25 °C. The 0.125 g/L of magnetic hydrochar catalyst and 200 mg/L TC solution was used to finish this experiment. The solution pH was adjusted with 1 mol/L HCl or NaOH. At first, to shield the adsorption effect of the catalyst, it is very necessary to fully shake the mixture of catalyst and TC solution for 1 h to reach adsorption equilibrium. In the meanwhile, a predetermined amount of peroxide hydrogen is added to trigger TC degradation. When arriving at a special time interval (namely 2, 2, 2, 2, 2, 5, 5, 10, 15, and 15 min), 1 mL solution was pressed through a 0.22 μm polyethersulfone filter and injected into a 2 mL centrifuge tube containing 0.1 mol/L $Na_2S_2O_3$ solution. The change in TC concentration in the different time-filtered samples was analyzed on a high-performance liquid chromatograph (Waters e2695, USA) at 357 nm. Mobile phase: methanol *vs.* 0.01 mol/L $(COOH)_2$ *vs.* acetonitrile = 8/72/20 (mL/mL/mL), flow speed: 1 mL/min, and injection volume: 20 μL were applied. The effects of different systems (biochar alone, hydrogen peroxide alone, biochar/H_2O_2), the ratio of reactant (the mass ratio of potassium ferrate and coconut fiber), H_2O_2 concentration (1.25–5 mmol/L), pH (3, 4, 5), biochar dosage (0.125–0.5 g/L), TC initial concentration (50–200 mg/L), anions (Cl^-, NO_3^-, $H_2PO_4^-$, HCO_3^-, SO_4^{2-}) and HA on TC oxidation degradation were explored. To study main active species participated in the degradation, scavenger agents such as MeOH, *tert*–butanol (TBA), *p*-benzoquinone (*p*-BQ), and L-histidine were added into the reaction system in a concentration ratio (1:50) of H_2O_2 to scavenger agent for scavenger experiments [15]. In addition, the electron spin resonance (ESR) spectra were applied to detect reactive oxygen species. More detailed experimental control conditions are shown in Table S1 (Supporting information). To ensure experimental reproducibility, all the oxidative degradation experiments were set up three parallel experiments, and the mean values were final representation.

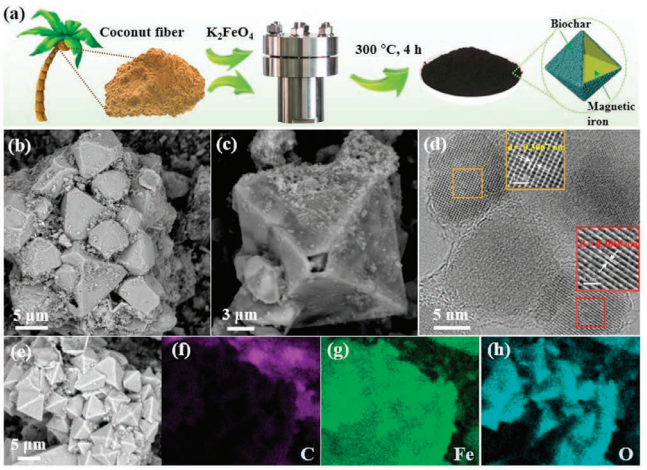


Fig. 1. (a) Preparation diagram of MHC. Scanning electron microscopy (SEM) images (b, c) and high resolution transmission electron microscopy (HRTEM) image (d) of MHC. (e–h) SEM image of MHC and corresponding energy-dispersive X-ray spectroscopy (EDS) mappings.

The preparation method of MHC is shown in Fig. 1a, wherein MHC was synthesized from coconut fibres and K_2FeO_4 using a simple hydrothermal carbonization method. The element composition and surface properties are listed in Table S2 (Supporting information). The MHC mainly consisted of C (19.02 %), H (1.31 %), O (27.53 %), and N (0.49 %) with Fe (43.63 %). The high contents of O and Fe revealed that iron oxides were massively doped and abundant oxygen-containing groups were generated. Fig. 1b demonstrates that iron oxide predominantly exhibits a regular octahedral structure, with biochar adhering to its surface. The elemental mapping diagram in Figs. 1e–h further proves that the octahedral struc-

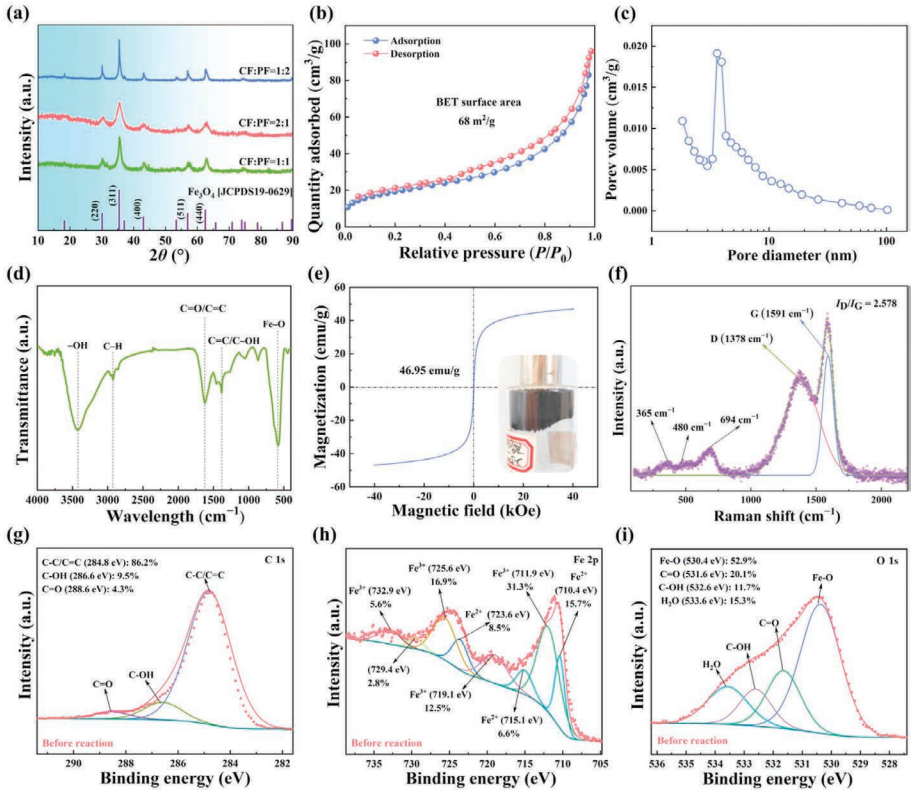


Fig. 2. (a) XRD patterns of MHC manufactured in different proportions. N_2-adsorption/desorption curves (b), pore size distribution (c), Fourier transform infrared-ray (FT-IR) spectrum (d), hysteresis curve (e), and Raman spectrum (f) of MHC. (f) X-ray photoelectron spectroscopy (XPS) spectra of C 1s (g), Fe 2p (h) O 1s (i) of MHC.

ture is iron oxide. The interior of the octahedra contains a rich porous architecture, which was conducive to confinement catalysis for degradation of pollutants (Fig. 1c). Additionally, through ordered assembly, various morphological iron species, such as tetrahedral, oblong, tubular, and honeycomb, were also generated (Fig. S1 in Supporting information). These diverse shapes of iron species should be resulted from modulation of *in-situ* generated ligands such as carboxylic acids and alcohols during hydrothermal carbonization of coconut fiber [23]. These iron oxides would afford sufficient catalytic sites for Fenton-like degradation of pollutants.

The transmission electron microscopy (TEM) images showed that nano-cubic iron oxides were generated and loaded on carbon matrix to form nano-heterostructures (Fig. S2 in Supporting information), contributing greatly to catalyse the Fenton-like degradation [12]. The generation of polyhedral iron oxides might be resulted from modulation of oxygen-containing ligands on carbon matrix. These iron species should play an important role for accelerating Fenton-like degradation of pollutants. Especially, the nano-heterostructures of iron oxides and carbon matrix should serve as key active catalysis sites for Fenton-like degradation of pollutants, where Fe^{3+}/Fe^{2+} cycle could be accelerated by electron shuttle and transfer of carbon matrix. HRTEM characterization was further performed to identify magnetic iron species (Fig. 1d and Fig. S3 in Supporting information). 0.26 nm and 0.30 nm lattice spacings were observed, they should be assigned to the (311) plane of γ-Fe_2O_3 and the (220) plane of Fe_3O_4, respectively. Accordingly, both γ-Fe_2O_3 and Fe_3O_4 were main species doped onto the MHC. Additionally, a lattice spacing of 0.21 nm, assigned to (110) plane of nZVI [24], was also observed. Therefore, the magnetic iron species should be mostly consisted of γ-Fe_2O_3 and Fe_3O_4 with a small amount of nZVI on the MHC.

The X-ray diffraction (XRD) patterns showed five obvious peaks at 18.3°, 30.1°, 35.5°, 43.1°, 53.6°, 56.9°, 62.7°, and 74.1° on the magnetic hydrochars (Fig. 2a). They might be assigned to either γ-Fe_2O_3 and/or Fe_3O_4 [25]. These peaks decreased with reduction of K_2FeO_4 dosage from 1/1 g/g to 1/2 g/g. Expectedly, they significantly strengthened as enhancing the K_2FeO_4 dosage to 2/1 g/g. As a result, FeO_4^{2-} could be efficiently transferred into magnetic iron oxides by reduction of biomass during hydrothermal carbonization. Additionally, a weak peak around 44.5°, attributed to nZVI [26], was also detected on the MHC prepared using 1/1 g/g K_2FeO_4 dosage. The N_2-adsorption/desorption isotherms showed the MHC was type V porous material, and moderate specific surface area (67 m^2/g) was achieved with good pore volume (0.1484 cm^3/g) of mesopore structures (Figs. 2b and c). The abundant pore structures would provide mass transfer channel for adsorption and degradation of pollutants.

The FT-IR spectrum was described in Fig. 2d, the MHC possessed four main peaks around 3423, 1620, 1384, and 580 cm^{-1}, which could be belonged to –OH, C=O/C=C, C=C/aromatic OH, and Fe-O groups, respectively [27]. Obviously, the MHC was rich of –OH, benefiting to anchoring iron oxides and modulating redox properties for the degradation of pollutants. The strong Fe-O peak also demonstrated that large amounts of iron oxides were impregnated in the MHC. A high saturation magnetization (46.95 emu/g) was gained due to the massive impregnation of magnetic iron oxides (Fig. 2e), making it be magnetically separated after catalysis under acidic conditions. The Raman spectrum showed that three peaks around 365, 500 and 694 cm^{-1} were noticed on the MHC (Fig. 2f). These peaks could be attributed to Fe_3O_4 or γ-Fe_2O_3 [28–31]. This agreed well the characterization result of XRD. This clearly demonstrated FeO_4^{2-} was mostly reduced into magnetic Fe_3O_4 or γ-Fe_2O_3. Meanwhile, two strong bands around 1387 and 1591 cm^{-1} were observed, and were assigned to D and G bands of disorder and graphic sp^2 carbons, respectively. This suggested that highly aromatic structure was generated with abun-

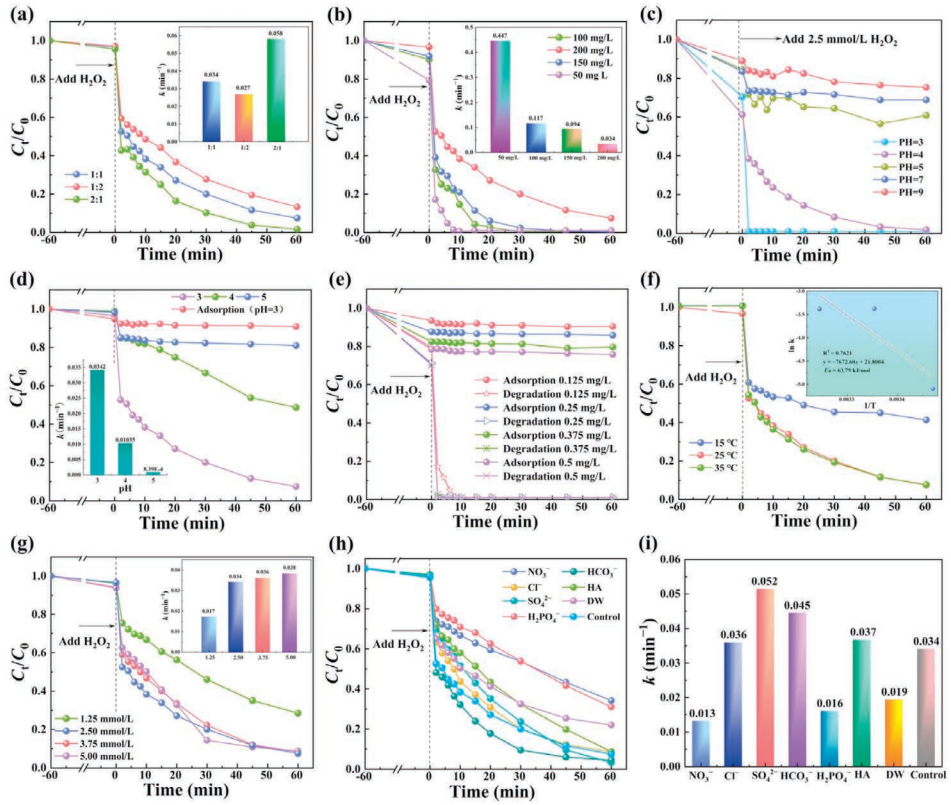


Fig. 3. (a) The catalysis performance of MHC prepared with different proportions; the inset is degradation rates. The effect of initial TC concentration (b), pH (c, d), dosage (e), temperature (f), H_2O_2 concentration (g), and co-existing anions (h, i) *via* MHC on Fenton-like degradation performance.

dant carbon defects by K_2FeO_4-promoted hydrothermal carbonization. These graphic structures should participate in the Fenton-like degradation by electron shuttle and transfer [25]. The D/G bands ratio was about 2.58, indicating abundant defects were generated. This was conducive to Fe^{3+}/Fe^{2+} cycle for activating H_2O_2 into ROSs by electron transfer and provider as well as activating H_2O_2 into ROSs directly [19].

The XPS spectra showed that the catalyst was mainly composed of C, O, and Fe, with surface concentrations of 67.7 %, 27.0 %, and 5.3 %, respectively (Fig. S4 in Supporting information), and N was almost undetectable. The C 1s spectra revealed 9.5 % –OH and 4.3 % C=O contents were observed (Fig. 2g), benefiting to anchoring iron oxides and boosting Fenton-like degradation for TC [32]. The deconvolution of Fe $2p_{1/2}$ spectrum led to two peaks at 710.4 and 711.9 eV, and that of Fe $2p_{3/2}$ spectrum resulted in two peaks at 723.6 and 725.6 eV [33]. The peaks at 710.4 and 723.6 eV were belonged to Fe^{2+}, and those at 711.9 and 725.6 eV were assigned to Fe^{3+} (Fig. 2h). Additionally, the satellite peaks of Fe^{2+} (715.1 eV, 729.4 eV) and that of Fe^{3+} (719.1 eV, 732.9 eV) were also observed for the MHC [34]. The ratios of the peaks of Fe^{2+} and Fe^{3+} were all around 1:2. Therefore, ferrous and ferric oxides were doped onto the surface of MHC. The O 1s peak was divided into four peaks around 530.4, 531.6, 532.6, and 533.6 eV which could be attributed to O-Fe, O=C, O-C, and H_2O, respectively, with 52.9 %, 20.1 %, 11.7 %, and 15.3 % (Fig. 2i). This suggested that abundant oxygen-containing groups were generated around iron oxides, which was conducive to accelerating Fe^{3+}/Fe^{2+} cycle for Fenton-like oxidation by electron shuttle and transfer [19,33].

The dosage of K_2FeO_4 was evaluated for improving the catalysis activity of magnetic hydrochar (Fig. 3a). As the ratio of K_2FeO_4 to coconut fiber increased from 1/1 g/g to 1/2 g/g, the catalysis activity of magnetic hydrochar reduced as low removal rate of TC (1/2: 88.6 % *vs.* 1/1: 92.5 %) was observed with lower TOC removal rate (1/2: 26 % *vs.* 1/1: 35 %) for a 50 mg/L concentration of TC (Fig. S5 in Supporting information). It should be noted that comparable adsorption capabilities for the MHC prepared with 1/2 and 1/1 ratios of K_2FeO_4 coconut fiber. While the ratio increased to 2/1 g/g, the degradation rate of TC was enhanced from 92.5 % to 98.3 % with enhancement of degradation constant from 0.034 min^{-1} to 0.058 min^{-1}. Whereas, the adsorption capacity decreased from 16.2 % to 11.7 % (Fig. S5 in Supporting information). Therefore, the catalysis performance strengthened, which could be contributed to introduction of more active catalysis sites. Moreover, the increase of oxygen-containing groups with electron transfer performance was also another reason for causing enhancement of oxidative degradation rate. However, the TOC removal rate comparable to that of 1/1 ratio (2/1: 37 % *vs.* 1/1: 35 %) due to comparable mineralization of intermediates and/or leaching of organic matters (2/1: 2.4 mg/L *vs.* 1/1: 1.5 mg/L) from the magnetic hydrochars (Fig. S6 in Supporting information). Therefore, the magnetic hydrochar manufactured with 1/1 ratio was employed to study Fenton-like degradation of TC.

The degradation of TC proceeded well over a concentration range of 50–200 mg/L, and the degradation rate slightly decreased from 99 % to 95 % slightly as the concentration rose from 50 mg/L to 200 mg/L (Fig. 3b). The degradation constant K_b decreased with TC concentration due to a limited amount of ROSs from activation of a certain amount of H_2O_2 in the catalysis system. Additionally, more active catalysis sites were covered by TC at high concentrations, leading to decreasing of catalysis efficiency. Importantly, the catalytic degradation of TC still underwent rapidly even at a concentration up to 200 mg/L, suggesting that most active catalysis sites were available for degradation of TC. As a result, the MHC showed good catalysis efficiency for the degradation of TC at different concentrations in this Fenton-like oxidation.

The pH could influence adsorption capability and catalysis activity as a crucial factor impacting the states of TC and surface chemical environment of magnetic hydrochar as well as Fe^{2+}/Fe^{3+} recycle for Fenton-like degradation and oxidizing ability of ROSs [35]. As shown in Fig. 3c, the MHC displayed enhanced adsorption capability as pH was enhanced from 3 to 4 at 50 mg/L concentration of TC. While pH rose to 5, the adsorption removal rate decreased from 29.6 % to 15.5 %. The degradation removal rate was up to 99 % at pH 3, and slightly declined to around 98 % at pH 4. The MHC still showed high catalysis performance at pH 4 even with more adsorption and coverage of TC on surface. Nevertheless, it remarkably decreased to 39 % even with lower adsorption capability while pH 5 was applied. Obviously, the catalysis activity was highest at pH 3, and somewhat declined at pH 4 with higher adsorption capability (comparable removal rate). This could be mainly attributed to reduction of Fe^{3+}/Fe^{2+} recycle and oxidizing ability of ROSs ($^{\bullet}OH$) at higher pH by persistent radical of carbon matrix (oxygen and carbon persistent radicals) [35]. In addition, Acidic conditions favor the catalytic role of Fe^{2+} in producing $^{\bullet}OH$ from H_2O_2, while also inhibiting the hydrolysis of Fe^{3+}, which can maintain a high level of iron ion concentration in the reaction system. In short, the degradation of TC proceeded rapidly at pH 3, and up to 99 % TC removal rate was achieved within 2 min with 35 % TOC removal rate after 60 min of degradation. To further distinguish the influence of initial pH, the Fenton-like degradation was examined using 200 mg/L over a pH range of 3–5 (Fig. 3d). Obviously, the degradation rate of TC sharply declined from 93 % to 19 % with from 0.0342 min^{-1} to 0.0003 min^{-1} as pH was enhanced from 3 to 5. As a result, the optimal pH was 3 for the Fenton-like degradation with catalysis of the MHC.

The MHC exhibited moderate adsorption capability toward TC, and its adsorption increased from 9.6 % to 24.2 % with dosage from 0.125 to 0.5 g/L at a 50 mg/L concentration (Fig. 3e). Considering the adsorption rate almost maintained constant after 60 min, and thereby the catalytic oxidative degradation was studied after adsorption equilibrium. TC could be mostly degraded using a dosage range of MHC from 0.125 g/L to 0.5 g/L with comparable removal rates (98.9 %–99 %). For example, the removal rates were 98.9 % and 99 % for 0.125 and 0.5 g/L, respectively. Importantly, high catalysis activity was still observed for 0.125 g/L dosage of magnetic hydrochar even its surface was covered by TC. As a result, a 0.125 g/L dosage of MHC guaranteed to efficiently accelerate the Fenton-like degradation of TC with low adsorption rate, and was used to investigate the following experiments.

The removal rate of TC was enhanced from 58.7 % to 92.5 % as degradation temperature rose from 15 °C to 25 °C, and the degradation constant k_d enlarged from 0.0061 min^{-1} to 0.0342 min^{-1} (Fig. 3f and Fig. S8 in Supporting information). This suggested that the Fenton-like degradation was an endothermic process for activating H_2O_2 into ROSs. According to the Arrhenius equation ($\ln k = \ln A - E_a/RT$), the activation energy of MHC was calculated to be 63.79 kJ/mol, indicating that an increase in temperature facilitates overcoming the reaction energy barrier, thereby accelerating the reaction rate (inset of Fig. 3f). While the degradation temperature was enhanced to 35 °C, and degradation rate constant rarely increased even ROSs exhibited stronger oxidizing ability at higher temperature. This could be ascribed to increasing H_2O_2 decomposition into nonreactive O_2 and H_2O at higher temperature [12]. Therefore, 25 °C was optimal temperature for Fenton-like degradation of TC in the catalysis system.

The removal efficiency was significantly improved when H_2O_2 concentration rose from 1.25 mmol/L to 2.5 mmol/L at 200 mg/L concentration of TC, where k_d rose from 0.017 min^{-1} to 0.038 min^{-1} (Fig. 3g). This could be ascribed to generation of more ROSs from H_2O_2 for the degradation of TC. While a higher concentration of H_2O_2 (3.75–5 mmol/L) was employed, the removal rate almost maintained unchanged as 2.5 mmol concentration with comparable k_d. This suggested that excessive H_2O_2 could not facilitate degradation due to conversion of H_2O_2 into nonactive O_2 and H_2O with catalysis of MHC [36]. Therefore, 2.5 mmol/L concentration of H_2O_2 was optimal for the degradation of TC with 0.125 g/L dosage of MHC, and H_2O_2 could be efficiently utilized for oxidative decomposition of TC in this catalysis system.

Co-existed anions might quench ROSs and inhibit Fe^{3+}/Fe^{2+} cycle in Fenton-like degradation [37]. The effect of anion was investigated using typical anions including Cl^-, HCO_3^-, HCO_3^-, SO_4^{2-}, NO_3^-, and $H_2PO_4^-$ at 50 mmol/L (Fig. 3h). The Cl^- rarely imposed influence on the catalysis of MHC for Fenton degradation of TC. HCO_3^- and SO_4^{2-} brought acceleration of TC degradation and the removal rate slightly rose from 92.5 % to 95.4 % and 96.7 %, respectively. The NO_3^- and $H_2PO_4^-$ led to obvious decrease in degradation rate and TC degradation efficiency reduced from 92.5 % to 65.8 % and 69 %, respectively, which could be ascribed to quenching of $^{\bullet}OH$ radical and co-precipitation of $FePO_4/Fe_3(PO_4)_2$, respectively. HA caused slight increase in degradation rate without increase of removal rate at 50 mg/L, demonstrating its great potential (Fig. 3i). Natural matters in DW caused remarkable reduction in degradation of TC owing to massive consumption of ROSs by them, and the removal rate decreased from 92.5 % to 78 %. These results suggested that the MHC could be a promising catalyst for promoting degradation of TC in wastewater.

The quenching experiments were conducted to identify ROSs for oxidation degradation of TC. Different reactive oxygen species trappers including MeOH, KI, FFA, L-histidine, and *p*-BQ (Fig. 4a) were used. The degradation efficiency reduced to 74.9 % and 63.3 % with MeOH and TBA, respectively, suggesting $^{\bullet}OH$ was involved in the degradation [38]. The $^{\bullet}OH$ should be generated from the homolysis of H_2O_2 activated by Fe^{2+}, PFRs, and oxygen-containing groups [39]. KI brought increase of degradation rate without reduction of removal rate, suggesting free $^{\bullet}OH$ contributed to degradation of TC rather $^{\bullet}OH$ binded on the surface of MHC [9]. This could be ascribed to low adsorption of $^{\bullet}OH$ on surface. The addition of *p*-BQ caused significant reduction of removal rate from 92.5 % to 23.3 %, indicating $^{\bullet}O_2^-$ was major ROSs in the catalysis system [36]. $^{\bullet}O_2^-$ ($HO_2^{\bullet}$) should be mainly resulted from the reaction of Fe^{3+} and H_2O_2 [39]. The degradation efficiency reduced from 92.5 % to 34 % with FFA, and thereby $^1O_2$ was also generated in the catalytic system and participated in the degradation as $^{\bullet}OH$. Additionally, L-histidine, a trapper of $^1O_2$, also caused decrease of degradation efficiency from 92.5 % to 29.8 %, further demonstrating that $^1O_2$ contributed greatly to the degradation of TC [40,41]. Accordingly, the contribution of ROSs followed the order: $^{\bullet}O_2^- > {}^1O_2 > {}^{\bullet}OH$ for degradation of TC, indicating that Fe^{3+} activate H_2O_2 into $^{\bullet}O_2^-$ was crucial for degradation of TC. The process of Fe^{3+} activating H_2O_2 to form $^{\bullet}O_2^-$ can be represented as: $Fe^{3+} + H_2O_2 \rightarrow H^+ + FeOOH^{2+} \rightarrow Fe^{2+} + HO_2^{\bullet} \rightarrow Fe^{2+} + H^+ + {}^{\bullet}O_2^-$ [42,43]. Therefore, the ROS generation process involved in the oxidative degradation of TC is as follows (Eqs. 1–9):

$$Fe^{2+} + H_2O_2 \rightarrow Fe^{3+} + {}^{\bullet}OH + OH^- \quad (1)$$

$$Fe^{3+} + H_2O_2 \rightarrow Fe^{2+} + HO_2^{\bullet} + H^+ \quad (2)$$

$$Fe^{3+} + HO_2^{\bullet} \rightarrow Fe^{2+} + H^+ + {}^1O_2 \quad (3)$$

$$HO_2^{\bullet} \rightarrow {}^{\bullet}O_2^- + H^+ \quad (4)$$

$$Fe^{2+} + HO_2^{\bullet} \rightarrow Fe^{3+} + HO_2^- \quad (5)$$

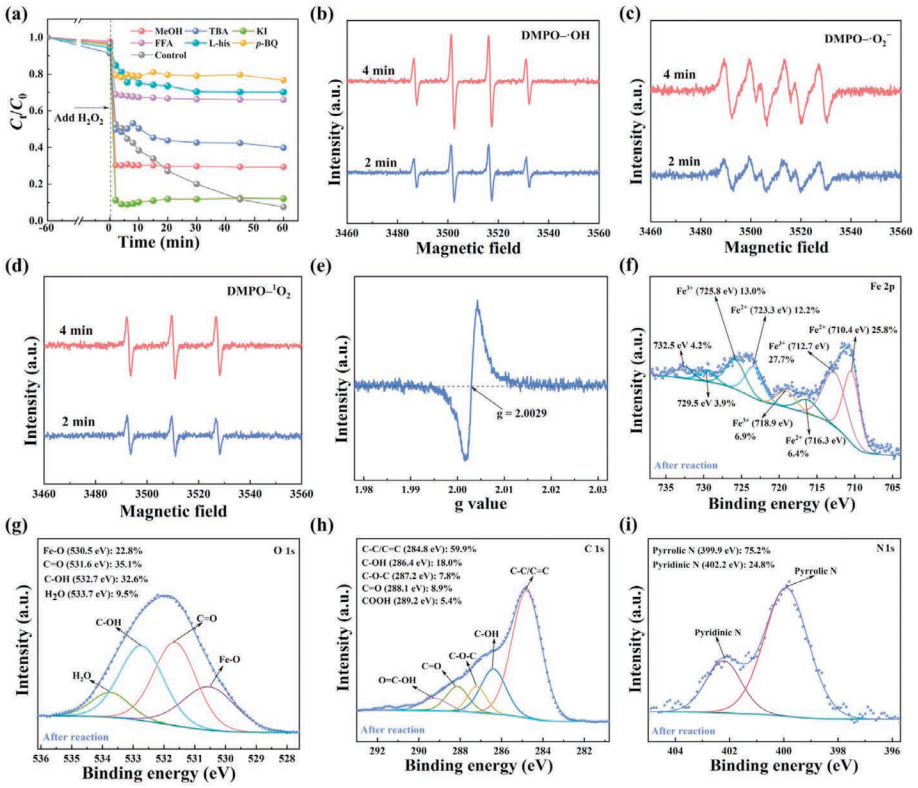


Fig. 4. (a) Active species quenching experiments. ESR spectra of $^{\cdot}O_2^-$ (b), $^{\cdot}OH$ (c), and $^1O_2$ (d) respectively. (e) ESR signals of MHC. XPS spectra of Fe 2p (f), O 1s (g), C 1s (h), and N 1s (i) of samples after reaction.

$$H_2O_2 + {}^{\cdot}OH \rightarrow HO_2^{\cdot} + H_2O \quad (6)$$

$$^{\cdot}O_2^- + HO_2^{\cdot} + H^+ \rightarrow H_2O_2 + {}^1O_2 \quad (7)$$

$$2{}^{\cdot}O_2^- + 2H_2O \rightarrow H_2O_2 + {}^1O_2 + 2HO^- \quad (8)$$

$$^{\cdot}O_2^- + {}^{\cdot}OH \rightarrow {}^1O_2 + HO^- \quad (9)$$

The ESR characterization was also performed to test ROSs in the Fenton-like system. As shown in Fig. 4b, a 1/2/2/1 ratio peaks were detected with DMPO, demonstrating the generation of $^{\cdot}OH$ in the catalysis system. Moreover, a 1/1/1/1 ratio peaks were also observed with DMPO, indicating the formation of $^{\cdot}O_2^-$ in the catalysis system (Fig. 4c). The trapping experiment of TEMP showed that triple peaks in a 1:1:1 ratio was detected, which should be resulted from its reaction with $^1O_2$ (Fig. 4d). As a result, $^{\cdot}OH$, $^{\cdot}O_2^-$, and $^1O_2$ were all generated in the catalysis system. Additionally, these ROSs increased with time from 2 min to 4 min. This agreed well with quenching experiments, further demonstrating these diverse active species were generated in this catalysis system and acted on oxidative degradation TC. The peak intensity of $^{\cdot}O_2^-$ was much stronger than that of $^1O_2$ and $^{\cdot}OH$, suggesting that $^{\cdot}O_2^-$ surpassed $^1O_2$ and $^{\cdot}OH$ for oxidative degradation of TC. This indicates that there is a process in the reaction system where Fe^{3+} activates H_2O_2 to generate $^{\cdot}O_2^-$, and this step is crucial for the MHC oxidation and degradation of TC. Moreover, the ESR spectra indicated that g factor was around 2.0029 (Fig. 4e), indicating that oxygen and carbon persistent radicals were generated on the MHC and could activate H_2O_2 into ROSs for the degradation [9]. Additionally, carbon matrix and oxygen functional groups could serve as redox sites for cycling Fe^{2+}/Fe^{3+}, benefiting to boosting activation of H_2O_2 into ROSs. Overall, carbon matrix synergistically worked with iron species besides serving as supporter for iron species.

The MHC was characterized by XPS spectra after catalytic degradation to identify the catalysis sites for the Fenton-like degradation. The XPS spectrum of Fe 2p indicated the ratio of $Fe^{2+}$to Fe^{3+} increased from 10/20 to 19/20, suggesting Fe^{2+}/Fe^{3+} cycle efficiently took place for activating oxidative degradation of TC (Fig. 4f). Moreover, oxygen content increased to 27.7 %, which could be mainly attributed to adsorption of oxidative degradation intermediates (Fig. 4g and Fig. S4 in Supporting information). C 1s spectrum indicated that oxygen-containing groups increased on the surface of MHC (Fig. 4h). N was detected on surface with 4.3 %, which could be ascribed to the adsorption of N-containing degradation intermediates on MHC (Fig. 4i). As a result, the adsorption of degradation intermediates should be contributed to removal of TOC. This would result in reduction of active catalysis sites with coverage of degradation intermediates on surface. Additionally, iron content obviously decreased on surface mainly ascribing to adsorption of degradation intermediates (Fig. S4 in Supporting information).

The MHC was characterized by SEM-EDS after catalytic oxidative degradation for two times. The iron content almost remained unchanged after degradation, demonstrating that iron and carbon matrix could remain stable during catalysis under acidic conditions (Table S3 in Supporting information). Agreeing well with XPS characterization result, SEM-EDS also showed that oxygen content also increased after degradation, further demonstrating adsorption of degradation intermediates on the MHC. This adsorption might occupy active catalysis sites, causing decrease of catalysis activity for the degradation of TC.

The MHC possessed abundant oxygen-containing groups and graphite structures with defects on carbon matrix. Therefore, car-

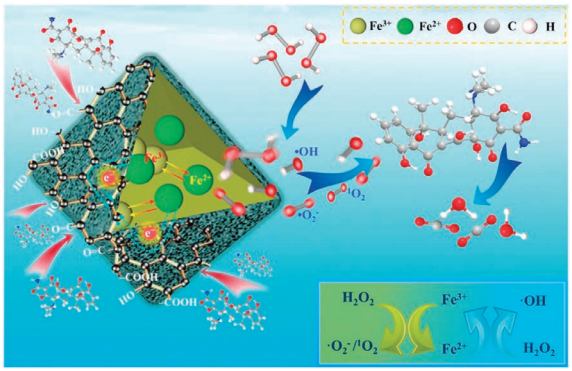


Fig. 5. The schematic diagram of synergy Fenton-like degradation in the MHC system.

bon matrix not only served as support for capturing and stabilizing iron oxides but also catalysis sites for the degradation of TC. Moreover, carbon matrix could accelerate Fe^{3+}/Fe^{2+} cycle with abundant oxygen-containing groups and graphite carbon by electron shuttle and transfer [19]. Therefore, carbon matrix synergistically collaborated with iron species for boosting the Fenton-like degradation of TC (Fig. 5).

The catalysis activity toward different oxidants was examined at a high concentration, the degradation efficiency was enhanced with peroxymonosulfate (PMS), and persulfate (PS) (Fig. 6a). The degradation efficiency followed the order: PMS > PS > H_2O_2, which was consistent with the oxidant potentials of these oxidants [12]. This revealed that the MHC was a versatile catalyst for activating different oxidants to generate ROSs for efficient degradation of TC. This would provide diverse oxidation reactions for elimination of TC from different aqueous environments.

The catalysis of MHC was also evaluated for degradation of other pollutants including SMX, SMR, and BPA (Fig. 6b). The adsorption capabilities followed by the order BPA > SMX > SMR. The catalysis degradation efficiency followed by the order SMX > BPA > SMR. In brief, good removal rates were obtained for SMX and BPA with simultaneous degradation and adsorption within 2 h. Comparatively, low removal rate was observed for SMR, this was consistent with previous reports in the literature [12,44]. This could be attributed to the relatively unstable five-membered oxazole ring in SMX, which contains N-O atoms; its loose electron cloud structure imparts higher reactivity. In contrast, SMR contains a six-membered heterocycle with two nitrogen atoms, resulting in a relatively stable structure, a more concentrated electron cloud distribution, and both symmetry and resonance stabilization. The MHC exhibited good degradation efficiency for different pollutants even at a high concentration (200 mg/L) with low dosage of MHC (0.125 mg/L).

To evaluate the potential application of MHC, the degradation of TC was studied in actual water matrices from Hongcheng lake, Nandu river, and tap water (Figs. 6c and d). The catalytic degradation efficiency almost maintained at the same level in tap water as ultrapure water, demonstrating limited minerals in tap water rarely influenced the degradation. In contrast, the degradation efficiency significantly reduced in Hongcheng lake and Nandu river water, but still maintained around 63.2 % and 70 %, respectively, demonstrating the great potential of MHC for efficient degradation of TC in practical applications. In the water matrices of Hongcheng lake and the Nandu river, a significant amount of organic matter is present, the MHC could serve as an effective candidate for mitigating organic pollution in these aquatic systems. Therefore, the catalysis system should contribute to degradation of the organic matter, causing reduction of degradation efficiency for TC. Additionally, the minerals in these natural waters could be adsorbed on the MHC, occupied and reduced active catalysis sites.

To assess recyclability of the MHC, it was simply separated by filtration and washed by a small amount of ultrapure water, and used for catalyzing degradation of TC directly. As shown in Fig. 6e, the catalysis efficiency slightly reduced for the first two times, and gradually reduced to 92.5 % after four times cycles. The adsorption capability also reduced from 9.8 % to 7.2 % as the MHC was cycled four times. These could be mainly ascribed to adsorption of molecular fragments on the MHC and occupation of active catalysis sites. This result was consistent with the observed increase of N and O content on the MHC as evidenced by XPS spectra (Figs. 4g–i). The FTIR spectra also showed that the peak of C=O strengthened with recycle, which should be resulted from adsorption of oxidative degradation intermediates (Fig. 6f). Moreover, the slight leaching of active iron oxides from the surface might also cause decrease of catalysis activity (Fig. 6g). Anyhow, this MHC should be recyclable with good catalysis activity.

The Fe leaching was analyzed in the catalysis system after degradation for evaluating the stability of MHC. The Fe dissolution was around 0.65 mg/L during adsorption under acidic conditions (Table S4 in Supporting information). The Fe leaching almost maintained unchanged while H_2O_2 concentration increased from 1.25 mmol/L to 5 mmol/L, indicating Fenton-like oxidation did not cause increased Fe leaching during degradation. The contribution of free iron oxides in aqueous solution to the Fenton-like oxidation reaction is limited due to their low concentration [45]. Even though high content of iron was doped onto MHC, only around 2.8 ‰ of Fe was released into aqueous solution. Comparing the XRD spectra of the catalyst before and after degradation reveals no significant changes in the XRD patterns of MHC, with the position and intensity of the diffraction peaks remaining consistent with those of the fresh sample, indicating that the MHC catalyst exhibits good stability (Fig. S9 in Supporting information). The FTIR spectra also demonstrated that Fe-O content rarely reduced after catalysis degradation (Fig. 6f). As a result, iron was mostly stably anchored on the carbon matrix with coordination of oxygen contained on carbon matrix and contributed greatly to catalytic degradation of TC.

The intermediates of the reaction process were identified by high-resolution mass spectra. A series of degradation intermediates were detected (Table S5 in Supporting information). Based on this result, there may be three degradation mechanisms as shown in Fig. 7. The ROSs including $^{\bullet}OH$, $^{\bullet}O_2^-$, and $^1O_2$ were generated for Fenton-like degradation of TC. These ROSs attacked TC molecules, resulting in deamination, dehydroxylation, demethylation, and ring-opening reactions to generate a series of intermediate products [46,47]. Pathway I: TC is gradually mineralized by demethylation, deamination, dehydroxylation, and ring-opening reaction through the attack of radicals. Pathway II: TC molecules are hydroxylated by adding a hydroxyl to hydroxylphenyl, and ring-opening reaction and functional group decomposition simultaneously occurred to produce smaller organic fragments, then finally mineralized into CO_2 and H_2O. Pathway III: hydroxylation reaction took place first, followed by deamination and dehydration reaction to become **III-P4** ($m/z = 394$), and then gradually decomposed and mineralized to H_2O and CO_2.

Given that the mineralization rate of TC was moderate than its removal rate, it is crucial to evaluate the potential toxicity of intermediates. In this study, the acute (LC_{50}) and chronic (ChV) toxicity of the molecular fragments generated during the degradation to freshwater organisms, such as water fleas, fish, and green algae, was assessed using the ECOSAR software [48]. The evaluation results are provided in Table S6 (Supporting information) [49]. As illustrated in Fig. 7d, the majority of intermediates are non-toxic toward fish, daphnia, and green algae, with only a few displaying

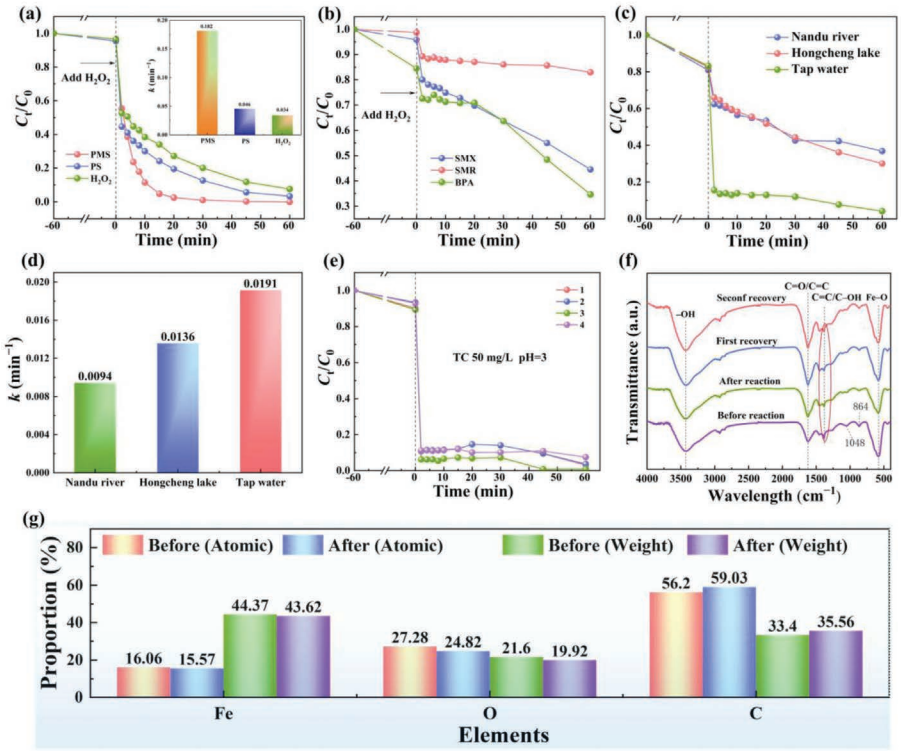


Fig. 6. (a) Effects of oxidants on MHC system. (b) The degradation effect of MHC on different pollutants. (c, d) The degradation of TC by MHC in different water matrices and the corresponding reaction rate. (e) Continuous cyclic degradation test. (f) FT-IR spectra of fresh and used samples. (g) The change of catalyst composition before and after reaction.

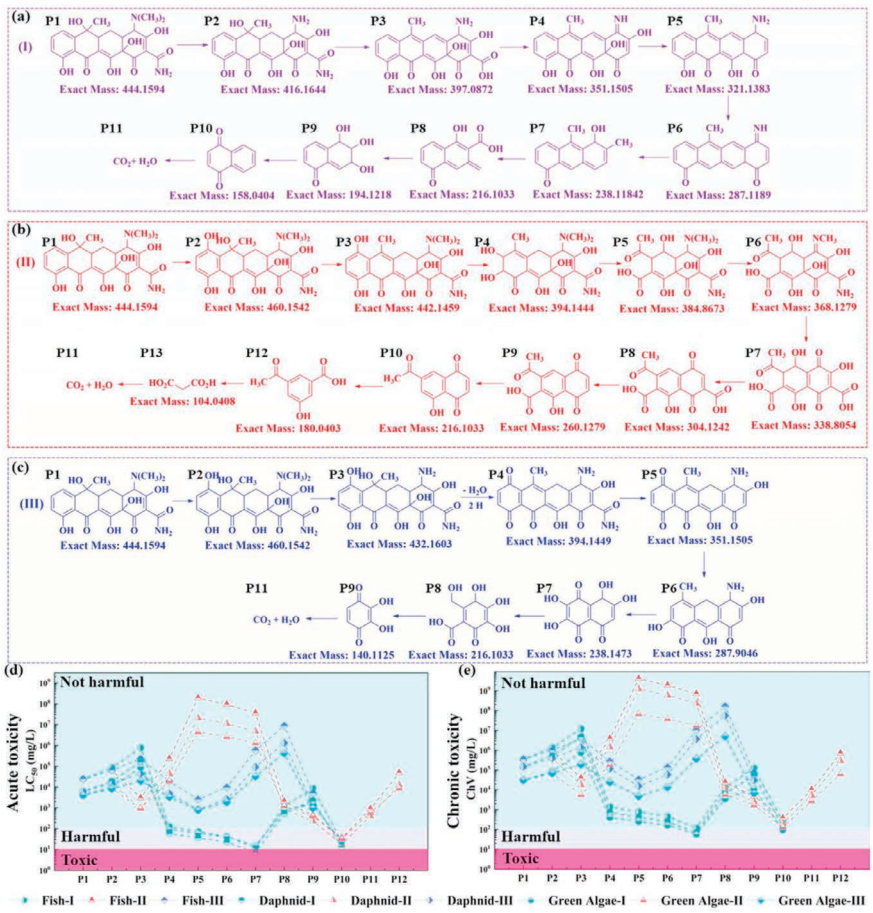


Fig. 7. (a–c) Degradation pathways of TC in the MHC system. Acute toxicity (d) and chronic toxicity (e) of degradation intermediates to daphnia, green algae, and fish.

harmful effects. Importantly, no toxic or highly toxic intermediates were detected. In degradation pathway I, however, intermediates such as **P4**, **P5**, **P6**, **P7**, and **P10**, which exhibited chronic toxicity, were identified. In contrast, the intermediates generated in pathways II and III are entirely non-toxic, with a notable reduction in overall toxicity. These findings indicate that all degradation intermediates pose no secondary environmental hazards. Additionally, phytotoxicity tests further elucidated the hazards posed by TC and its degradation intermediates. As shown in Table S7 (Supporting information), the TC solution before degradation significantly inhibited the germination of wheat, indicating that TC-contaminated water possesses high toxicity. In contrast, the inhibitory effect on wheat germination was markedly reduced after the degradation of TC, demonstrating a decrease in biological adverse impacts following degradation *via* the MHC system.

In summary, a high-performance MHC was manufactured simple K_2FeO_4-promoted hydrothermal carbonization for catalytic oxidative degradation of tetracycline in aqueous solution. Diverse shapes of iron oxides were doped on carbon matrix with abundant oxygen functional groups. Especially, tunable and channel structure of iron species were constructed with regulation of *in-situ* generated ligands for confine catalyzing the Fenton-like degradation. Moreover, the nano-heterojunction structure of carbon matrix and iron oxides was generated and acted as key active catalysis sites for spitting H_2O_2 into active species for degradation of TC. Furthermore, abundant carbon defects were created with persistent free radicals, which was also conductive to Fenton-like degradation as catalyst and activator of Fe^{3+}/Fe^{2+} cycle. The MHC stably survived during oxidative degradation with less release of iron, and good recyclability was achieved. The MHC exhibited high catalysis activity for the degradation of different types of pollutants and advanced oxidation processes.

Declaration of competing interest

The authors declare that they have no known competing financial interests or personal relationships that could have appeared to influence the work reported in this paper.

CRediT authorship contribution statement

Zijing Guo: Writing – original draft, Validation, Investigation, Data curation. **Yi Liang:** Investigation, Data curation. **Kaili He:** Visualization. **Hongru Jiang:** Supervision, Formal analysis. **Xiang Liu:** Supervision, Resources. **Congying Xu:** Supervision. **Yawei Xiao:** Writing – review & editing, Visualization, Project administration, Methodology. **Jihui Li:** Writing – review & editing, Supervision, Project administration, Methodology, Funding acquisition, Conceptualization.

Acknowledgments

This work was financially supported by Hainan Provincial Natural Science Foundation of China (Nos. 422RC600, 519QN175), National Natural Science Foundation of China (Nos. 52160018, 21801053, 52400206, 52500209), and High-Level Talent Program of Hainan Province (Nos. XJ2400008202, XJ2400011473).

Supplementary materials

Supplementary material associated with this article can be found, in the online version, at doi:10.1016/j.cclet.2025.111306.

References

[1] Y. Mao, B. Yu, P. Wang, S. Yue, S. Zhan, Nat. Commun. 15 (2024) 6364.
[2] M. Chen, J. Jiang, W. Guan, et al., Adv. Mater. 36 (2024) 2311416.
[3] J. Xu, Q. Zhang, X. Gao, et al., Angew. Chem. Int. Ed. 62 (2023) e202307018.
[4] H. Zhou, J. Peng, X. Duan, et al., Environ. Sci. Technol. 57 (2023) 3334–3344.
[5] H. Liu, M. Cheng, Y. Liu, et al., Sep. Purif. Technol. 355 (2025) 129659.
[6] L. Wang, L. Rao, M. Ran, et al., Nat. Commun. 14 (2023) 7841.
[7] W. Xia, S. Li, G. Wu, J. Ma, J. Hazard. Mater. 460 (2023) 132377.
[8] G. Zhou, F. Gao, T. Liu, et al., Adv. Funct. Mater. 34 (2024) 2406329.
[9] Y. Shen, Y. Xiao, H. Zhang, et al., Chem. Eng. J. 477 (2023) 146823.
[10] C. Zhou, M. Sun, P. Zhang, et al., J. Hazard. Mater. 476 (2024) 134979.
[11] S. Ye, G. Zeng, X. Tan, et al., Appl. Catal. B: Environ. Energy 269 (2020) 118850.
[12] Z. Feng, R. Yuan, F. Wang, et al., Sci. Total Environ. 765 (2021) 142673.
[13] W. Xiao, A. Chen, M. Cheng, et al., Water Res. 268 (2025) 122735.
[14] J. Qu, J. Shi, Y. Wang, et al., J. Hazard. Mater. 434 (2022) 128841.
[15] L. Li, C. Lai, F. Huang, et al., Water Res. 160 (2019) 238–248.
[16] L. Li, S. Liu, M. Cheng, et al., J. Hazard. Mater. 406 (2021) 124333.
[17] H. Qi, G. Pan, X. Shi, Z. Sun, Chem. Eng. J. 434 (2022) 134675.
[18] B. Shen, Y. Liu, S. Liu, et al., Process Saf. Environ. Prot. 144 (2020) 143–157.
[19] A. Chen, M. Heng, G. Wang, et al., Sep. Purif. Technol. 354 (2025) 129432.
[20] K. Luo, Q. Yang, Y. Pang, et al., Chem. Eng. J. 374 (2019) 520–530.
[21] X. Li, J. Xu, Z. Yang, Chem. Eng. J. 450 (2022) 1384666.
[22] Z. Guo, X. Chen, J. Hang, et al., Bioresour. Technol. 387 (2023) 129572.
[23] M.V. Kovalenko, M.I. Bodnarchuk, R.T. Lechner, et al., J. Am. Chem. Soc. 129 (2007) 6352–6353.
[24] H. Lv, H. Niu, X. Zhao, Y. Cai, F. Wu, Appl. Catal. B: Environ. Energy 286 (2021) 119940.
[25] H. Wu, G. Wu, L. Wang, Powder Technol. 269 (2015) 443–451.
[26] J. Deng, H. Dong, C. Zhang, et al., Sep. Purif. Technol. 202 (2018) 130–137.
[27] Y. Xiao, Z. wang, B. Yao, et al., Small 20 (2024) 2304843.
[28] Y.S. Li, J.S. Church, A.L. Woodhead, J. Magn. Magn. Mater. 324 (2012) 1543–1550.
[29] J. Zhang, P. Tan, W. Zhao, J. Lu, J. Zhao, J. Raman Spectrosc. 42 (2011) 1388–1391.
[30] Y. El Mendili, J.F. Bardeau, N. Randrianantoandro, et al., J. Raman Spectrosc. 42 (2011) 239–242.
[31] S. Babay, T. Mhiri, M. Toumi, J. Mol. Struct. 1085 (2015) 286–293.
[32] X. Li, K. Cui, Z. Guo, et al., Chem. Eng. J. 379 (2020) 122324.
[33] Z. Feng, X. Zhai, T. Sun, Sep. Purif. Technol. 293 (2022) 121120.
[34] Y. Liu, S.P. Sohi, S. Liu, et al., J. Environ. Manag. 235 (2019) 276–281.
[35] T. Luo, H. Feng, L. Tang, et al., Chen, Chem. Eng. J. 382 (2020) 122970.
[36] S. Xin, G. Liu, X. Ma, et al., Appl. Catal. B: Environ. Energy 280 (2021) 119386.
[37] C. Zhou, Y. Guo, S. Du, M. Sui, Appl. Catal. B: Environ. Energy 358 (2024) 124442.
[38] Y. Xiao, H. Li, B. Yao, et al., Chem. Eng. J. 484 (2024) 149399.
[39] L. Li, Z. Yin, M. Cheng, et al., Chem. Eng. J. 454 (2023) 140126.
[40] J. Tan, J. Wang, Z. Tan, et al., Chem. Eng. J. 451 (2023) 138504.
[41] Y. Yin, Y. Ren, J. Lu, et al., Appl. Catal. B: Environ. Energy 286 (2021) 119943.
[42] C. Walling, Acc. Chem. Res. 8 (1975) 125–131.
[43] X. Li, Y. Jia, J. Zhang, et al., Chin. Chem. Lett. 33 (2022) 2105–2110.
[44] Y. Li, J. Zhang, D. Cheng, et al., J. Environ. Manag. 366 (2024) 121872.
[45] C. Lai, X. Shi, L. Li, et al., Sci. Total Environ. 775 (2021) 145850.
[46] B. Yan, J. Peng, F. Deng, et al., Chem. Eng. J. 452 (2023) 139353.
[47] J. Ni, D. Liu, W. Wang, et al., Chem. Eng. J. 419 (2021) 129969.
[48] L. Wang, X. Lu, G. Chen, Y. Zhao, S. Wang, Chem. Eng. J. 468 (2023) 143773.
[49] S. Deng, X. Han, N. Lv, et al., Chem. Eng. J. 486 (2024) 150263.